

# Polaronic Enhancement of Second-Harmonic Generation in Lithium Niobate

Agnieszka L. Kozub,<sup>1,\*</sup> Arno Schindlmayr,<sup>1</sup> Uwe Gerstmann,<sup>1</sup> and Wolf Gero Schmidt<sup>1</sup>

<sup>1</sup>Universität Paderborn, Department Physik, 33095 Paderborn, Germany

(Dated: June 3, 2021)

Density-functional theory within a Berry-phase formulation of the dynamical polarization is used to determine the second-order susceptibility  $\chi^{(2)}$  of lithium niobate ( $\text{LiNbO}_3$ ). Defect trapped polarons and bipolarons are found to strongly enhance the nonlinear susceptibility of the material, in particular if localized at  $\text{Nb}_V\text{-V}_{\text{Li}}$  defect pairs. This is essentially a consequence of the polaronic excitation resulting in relaxation-induced gap states. The occupation of these levels leads to strongly enhanced  $\chi^{(2)}$  coefficients and allows for the spatial and transient modification of the second-harmonic generation of macroscopic samples.

The arbitrary control of electromagnetic waves is a key aim of photonic research. This requires the engineering of optical coefficients, e.g., by doping, strain, or electric fields [1–4]. Photorefractive materials like lithium niobate ( $\text{LiNbO}_3$ , LN) that respond to light by altering their refractive index are of particular interest in this context [5, 6]. Lithium niobate is used, e.g., for optical waveguides, optical modulators, photonic integrated circuits and nonvolatile holographic storage [7, 8].

deficit observed in the congruently melting composition of lithium niobate. Single polarons (F and P) are usually found as metastable states upon optical excitation and may combine to bipolarons. The latter also result from thermal or electrochemical reduction and can be thermally or optically split into single electron polarons [9, 11, 14]. Optical absorption peaks at about 0.9 eV, 1.6 eV, and 2.5 eV are assigned to F [15], P [16], and B polarons [17], respectively.

Controlling second-harmonic generation (SHG) in lithium niobate, i.e., the generation of new photons with twice the energy of the initial photons, requires engineering the second-order susceptibility  $\chi^{(2)}$  [18–20]. Although polarons have been known for a long time to cause various optical nonlinearities, such as green-induced infrared absorption [21], their influence on  $\chi^{(2)}$  is essentially unknown. In this Letter, we show by means of first-principles calculations that electron polarons cause a strong enhancement of the  $\chi^{(2)}$  susceptibility for photon energies in the lower half of the LN band gap and thus provide a means to control SHG in space and time.

In detail, we perform density-functional theory (DFT) electronic-structure calculations based on the Quantum Espresso [22, 23] implementation. The generalized gradient approximation is employed using the PBEsol functional. The nonlinear susceptibilities are obtained from the real-time evolution of the Bloch electrons in a uniform time-dependent electric field following the Berry-phase approach proposed by Attaccalite and Grüning [24].

Stoichiometric LN crystallizes in a rhombohedral unit cell. Oxygen atoms form octahedra that are alternately occupied by Li, Nb, or are empty, see Fig. 2(a). The present polaron calculations are based on previously established models [25], which account for both the measured optical absorption peaks and the electron paramagnetic resonance data. As shown in Fig. 2, we consider (a) free polarons, where the excess electron is bound to a regular  $\text{Nb}_{\text{Nb}}$  ion, (b) bound polarons with the excess electron at the  $\text{Nb}_{\text{Li}}$  antisite defect, (c) bound polarons with the excess electron at the Nb interstitial of the  $\text{Nb}_V\text{-V}_{\text{Li}}$  defect pair and bipolarons, where one of the excess electrons is at the defect niobium atom of (d) the  $\text{Nb}_{\text{Li}}$

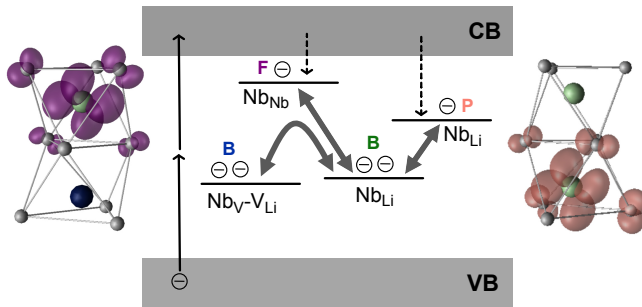


FIG. 1. (Color online) Schematic illustration of electron polaron states in lithium niobate. Band-to-band excitation and subsequent carrier localization result in the formation of free (F) and bound (P) polarons, which combine to bipolarons (B). Bipolarons may transform structurally or dissociate into single electron polarons. Charge densities of the polaron orbitals are shown on the sides: free polaron (left) and bound polaron (right), both in tilted ground state configuration.. See Fig. 2 for complete structures and the notation of atoms.

The LN optical properties are profoundly affected by polarons, i.e., electrons excited to a state close to the edge of the conduction band that get dressed with a cloud of virtual polar phonons [9–13]. Free small polarons (F) are the simplest polaron species in LN, see Fig. 1. They are formed by extra electrons stabilized at regular  $\text{Nb}_{\text{Nb}}$  ions of the LN lattice. Bound polarons (P) and bound bipolarons (B) are formed by single electrons and pairs of electrons, respectively, localized at point defects. These defects are related to excess Nb compensating the lithium

\* agnieszka.kozub@upb.de

antisite defect or (e) the  $\text{Nb}_V\text{-V}_{\text{Li}}$  defect pair, and the second one is at the neighboring Nb atom. The structures shown in (a), (b), and (c) are studied in both the axially symmetric and quasi-Jahn-Teller distorted (tilted) configurations [25]. The structures (d) and (e) have axial symmetry. In this case, the niobium atoms carrying the excess electrons shift along the crystal  $z$  axis preserving the threefold rotational symmetry. In the tilted configurations, the polaron-carrying atoms are shifted in the  $xy$  plane, which results in clover-leave like orbitals for the excess electrons [25]. The defect structures are modeled with 80-atom supercells, as described in Ref. [26]. Here, a  $3\times 3\times 3$   $\Gamma$ -centred  $\mathbf{k}$ -point sampling is used for the  $\chi^{(2)}$  calculations. The bulk LN calculations are performed using the 10-atom unit cell and a  $6\times 6\times 6$   $\Gamma$ -centred  $\mathbf{k}$ -point grid to determine  $\chi^{(2)}$ .

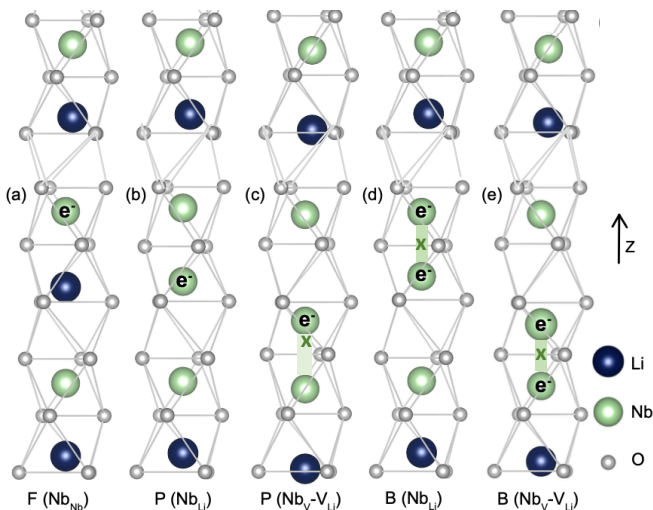


FIG. 2. (Color online) Free polarons (a), bound polarons (b, c), and bipolarons (d, e) in  $\text{LiNbO}_3$  defect structures. Trapped electrons ( $e^-$ ) as well as their hybridization along the  $z$ -axis and the center of the polaronic charges ( $x$ ) are indicated (cf. Fig. 3).

Fig. 3 shows the modulus of calculated second-order susceptibility tensor elements in dependence on the incident photon energy. Unless stated otherwise, we plot the most frequently measured value  $|\chi_{zzz}^{(2)}(\omega)|$ . The calculations for the stoichiometric bulk material agree well with previous calculations [27] and reproduce the order of magnitude of the measured data [28]. The low  $|\chi_{zzz}^{(2)}(\omega)|$  values for energies in the lower half of the LN band gap are strongly enhanced upon bipolaron formation and for  $\text{P}(\text{Nb}_V\text{-V}_{\text{Li}})$  with the axial symmetry. In the case of  $\text{B}(\text{Nb}_V\text{-V}_{\text{Li}})$ , where the enhancement is most pronounced, we also show the other second-order susceptibility tensor elements that are nonzero in trigonal symmetry [29], as e.g. present for stoichiometric LN as well as for the polaron states with axial symmetry:  $|\chi_{yxx}^{(2)}(\omega)|$ ,  $|\chi_{yyz}^{(2)}(\omega)|$ , and  $|\chi_{zxx}^{(2)}(\omega)|$  in Fig. 3. The latter are far

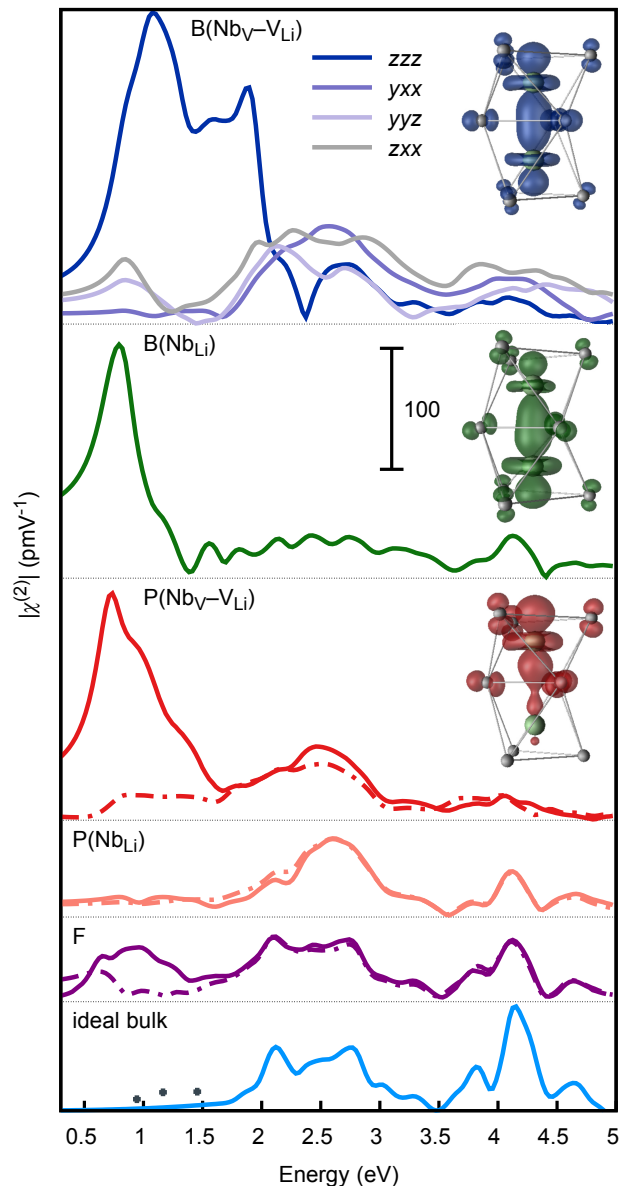


FIG. 3. (Color online) Values of  $|\chi^{(2)}(\omega)|$  calculated for ideal, stoichiometric LN as well as for supercells that contain electron polarons. Solid lines correspond to the structures with the axial symmetry, dashed lines to the tilted configuration. Black symbols in the bottom represent experimental data for congruent  $\text{LiNbO}_3$  [28].

smaller than  $|\chi_{zzz}^{(2)}(\omega)|$  in the low-energy region.

A common feature of all the systems with strongly enhanced  $|\chi_{zzz}^{(2)}(\omega)|$  is a pronounced hybridization of the polaron orbital at the defect niobium atom with the neighbouring atom along the  $z$  direction (see insets in Fig. 3). This hybridization shifts the center of the polaronic charge away from its position in ideal stoichiometric LN.

According to Miller's rule [18, 30], the quantity  $\Delta(\omega) = \chi^{(2)}(2\omega) / \{\chi^{(1)}(2\omega)[\chi^{(1)}(\omega)]^2\}$  is a slowly varying function of  $\omega$ . It accounts for frequency-doubling and allows

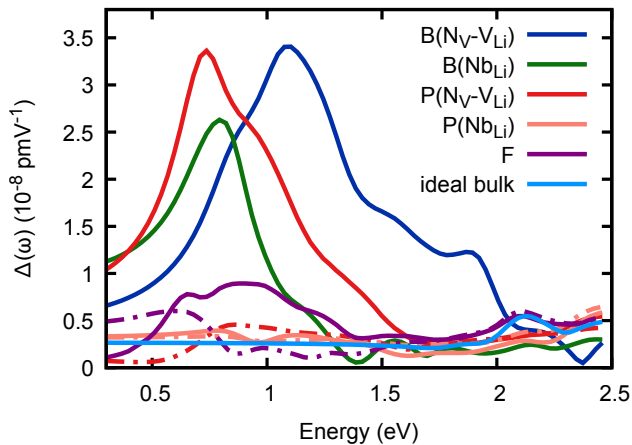


FIG. 4. (Color online) Check of Miller’s rule for bulk  $\text{LiNbO}_3$  as well as crystal structures containing electron polarons.

in many cases to relate linear and nonlinear susceptibilities of noncentrosymmetric crystals. As can be seen in Fig. 4, Miller’s rule holds indeed for stoichiometric LN but is clearly violated for bipolarons and  $\text{Nb}_V\text{-V}_{\text{Li}}$  localized bound polarons. Obviously, these systems are characterized by a strong bond charge acentricity and are not well described within the classical anharmonic oscillator model [18, 31]. In fact, the  $\chi^{(2)}$  values calculated here for the polaron or bipolaron containing supercells, i.e.,  $|\chi_{zzz}^{(2)}| \approx 200 \text{ pmV}^{-1}$  within the region of the LN band gap, are comparable to the value of GaAs in the energy region above the band gap, which is known as one of the largest  $\chi^{(2)}$  values reported for solid state systems [18].

*What is the microscopic origin of the large optical nonlinearities associated with some polaron species?* In order to answer this question we separate the influence of the defect formation and of the polaronic excitation, i.e., the trapping of additional electrons and of the associated lattice relaxation for the cases of the bipolarons as well as  $\text{P}(\text{Nb}_V\text{-V}_{\text{Li}})$ . In Fig. 5 it can be seen that the point defects themselves only slightly modify the  $|\chi_{zzz}^{(2)}|$  bulk values, at least for low photon energies. However, upon polaronic excitation the low-energy susceptibility is much enhanced, in analogy to the polaron-related additional absorption peaks in the linear optical response [15–17]. This enhancement can either be due to electronic transitions related to the polaron states, or it may be caused by the lattice relaxation accompanying the polaron formation. To discriminate between these two possibilities we perform calculations for supercells that model the (bi)polaron geometries, but do not contain the corresponding electrons. The corresponding spectra are plotted with dashed lines in Fig. 5. It can be seen that in the case of bipolarons both electronic occupation and lattice relaxation contribute to the  $\chi^{(2)}$  enhancement, while the electronic effects are dominant for bound polarons. For

$\text{B}(\text{Nb}_V\text{-V}_{\text{Li}})$  the SHG enhancement is not restricted to the spectral region around 1 eV, but extends to energies up to 2 eV, where an additional second peak can be identified. This peak is related to transitions into empty Nb  $4d$  states close the conduction-band edge and be already identified in the  $\text{B}(\text{Nb}_V\text{-V}_{\text{Li}})$  linear optical response [26]. Indeed, it well predicted already from Miller’s rule applied to  $\chi^{(1)}$  calculated for  $\text{B}(\text{Nb}_V\text{-V}_{\text{Li}})$ . This is shown by the black dashed line in Fig. 5.

*How important will the polaronic SHG enhancement effect be for real samples?* Merschjann and co-workers [32] determined polaron densities in congruently melting  $\text{LiNbO}_3$  by time-resolved pump–multiprobe spectroscopy. They obtained a steady-state number density of bipolarons of  $6.7 \times 10^{23} \text{ m}^{-3}$  at room temperature without illumination. The polaron density can be drastically enhanced by optical excitation. Electron polarons in lithium niobate are generated optically within a few hundred femtoseconds [33, 34]. Thereby concentrations far higher than in the steady state can be achieved. Buse

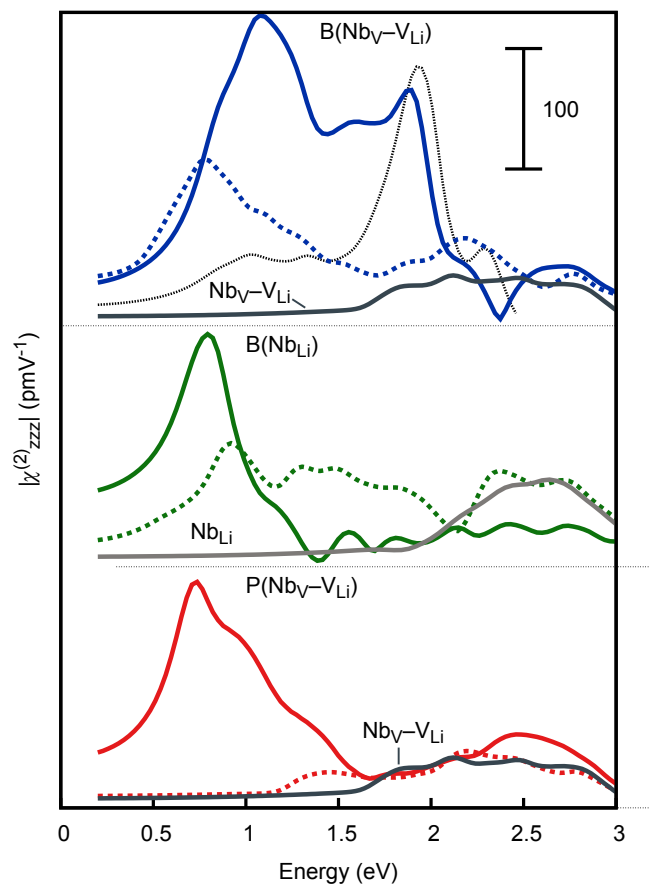


FIG. 5. (Color online)  $|\chi_{zzz}^{(2)}(\omega)|$  calculated for supercells containing defects, defect localized (bi)polarons, and (shown with colored dashed lines) polaronic structures without trapped electrons. The black dashed line represents  $|\chi_{zzz}^{(2)}(\omega)|$  estimated from Miller’s rule for  $\text{B}(\text{Nb}_V\text{-V}_{\text{Li}})$ .

*et al.* [33], for example, determine a polaron density of  $4.4 \times 10^{24} \text{ m}^{-3}$ . This value is used for an order-of-magnitude estimate for the bipolaron induced  $|\chi_{zzz}^{(2)}(\omega)|$  change in Fig. 6. Obviously,  $|\chi_{zzz}^{(2)}|$  changes of the order of a few percent can be expected to result from optical excitation of real samples.

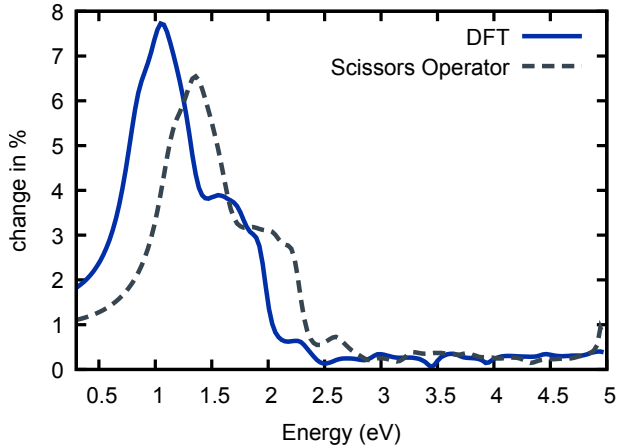


FIG. 6. (Color online) Relative change in  $|\chi_{zzz}^{(2)}(\omega)|$  due to  $B(\text{Nb}_V\text{-V}_{\text{Li}})$  formation in bulk  $\text{LiNbO}_3$ , assuming a density of  $4.4 \times 10^{24} \text{ m}^{-3}$ . In addition to calculations within the independent-particle approximation (DFT) also an estimate for the influence of self-energy corrections (Scissors Operator) is shown, see text.

A word of caution is in order considering the present DFT calculation. Optical excitations are known to be influenced by electronic many-body effects beyond DFT [35–41]. In order to probe their influence, a scissors operator correction is added to the effective Hamiltonian for the Bloch electrons. Its size has been determined by *GW* calculations [25] that predict a blueshift of 0.6 eV for transitions from the  $B(\text{Nb}_V\text{-V}_{\text{Li}})$  polaron state to the LN conduction band minimum compared to the DFT calculations. As expected, the self-energy effects lead to a blueshift and weakening of the SHG signal. As excitonic effects are expected to redshift and increase the SHG spectral features [35–38], the dashed line in Fig. 6 represents an upper limit for the excitation energies and a lower limit for the SHG enhancement that can be expected to result from the bipolaron formation. Obviously, the polaronic effect on  $\chi^{(2)}$  predicted here from DFT is robust with respect to many-body effects.

In summary, the present density-functional calculations predict a strong  $\chi^{(2)}$  enhancement in lithium niobate upon formation of bound (bi)polarens. It is caused primarily by the occupation of the relaxation-induced polaronic defect levels in the gap. Further details of the SHG enhancement depend sensitively on the relative position of the polaronic charge density with respect to the neighboring cations of the ferroelectric host material. The polaron density in real samples de-

pends (i) on the availability of possible lattice trapping sites – that may be locally modified by doping [9] – and (ii) can be strongly increased by optical excitation of the sample. The polaronic enhancement of the nonlinear optical coefficients predicted here thus suggests a novel way to control second-harmonic generation in space and time beyond strain or external electric field induced effects.

The DFG (TRR 142, project number 231447078) is acknowledged for financial support. We thank the Paderborn Center for Parallel Computing (PC<sup>2</sup>) and the Höchstleistungs-Rechenzentrum Stuttgart (HLRS) for grants of high-performance computer time.

- 
- [1] M. Cazzanelli, F. Bianco, E. Borga, G. Pucker, M. Ghulinyan, E. Degoli, E. Luppi, V. Véniard, S. Ossicini, D. Modotto, S. Wabnitz, R. Pierobon, and L. Pavesi, *Nature Materials* **11**, 148 (2012).
  - [2] R. S. Jacobsen, K. N. Andersen, P. I. Borel, J. Fage-Pedersen, L. H. Frandsen, O. Hansen, M. Kristensen, A. V. Lavrinenko, G. Moulin, H. Ou, C. Peucheret, B. Zsigri, and A. Bjarklev, *Nature* **441**, 199 (2006).
  - [3] K. L. Seyler, J. R. Schaibley, P. Gong, P. Rivera, A. M. Jones, S. Wu, J. Yan, D. G. Mandrus, W. Yao, and X. Xu, *Nature Nanotechnology* **10**, 407 (2015).
  - [4] J.-M. Yi, D. Wang, F. Schwarz, J. Zhong, A. Chimeh, A. Korte, J. Zhan, P. Schaaf, E. Runge, and C. Lienau, *ACS Photonics* **6**, 2779 (2019).
  - [5] J. Frejlich, *Photorefractive materials: Fundamental concepts, holographic recording and materials characterization* (Wiley, New Jersey, 2006).
  - [6] P. Günter and J. P. Huignard, eds., *Photorefractive Materials and Their Applications I: Fundamental Phenomena* (Springer, New York, 2014).
  - [7] L. Hesselink, S. S. Orlov, A. Liu, A. Akella, D. Lande, and R. R. Neurgaonkar, *Science* **282**, 1089 (1998).
  - [8] K. Buse, A. Adibi, and D. Psaltis, *Nature* **393**, 665 (1998).
  - [9] O. F. Schirmer, M. Imlau, C. Merschjann, and B. Schoke, *J. Phys: Condens. Matter* **21**, 123201 (2009).
  - [10] F. Luedtke, K. Buse, and B. Sturman, *Phys. Rev. Lett.* **109**, 026603 (2012).
  - [11] M. Imlau, H. Badorreck, and C. Merschjann, *Applied Physics Reviews* **2**, 040606 (2015).
  - [12] A. Krampf, S. Messerschmidt, and M. Imlau, *Sci. Rep.* **10**, 1 (2020).
  - [13] Y. Furukawa, M. Sato, K. Kitamura, Y. Yajima, and M. Minakata, *Journal of Applied Physics* **72**, 3250 (1992).
  - [14] C. Merschjann, D. Berben, M. Imlau, and M. Wöhlecke, *Phys. Rev. Lett.* **96**, 186404 (2006).
  - [15] B. Faust, H. Müller, and O. F. Schirmer, *Ferroelectrics* **153**, 297 (1994).
  - [16] K. L. Sweeney and L. E. Halliburton, *Applied Physics Letters* **43**, 336 (1983).
  - [17] J. Koppitz, O. F. Schirmer, and A. I. Kuznetsov, *Europhysics Letters (EPL)* **4**, 1055 (1987).

- [18] R. W. Boyd, *Nonlinear Optics* (Academic Press, London, 2020).
- [19] J. E. Sipe and A. I. Shkrebtii, *Phys. Rev. B* **61**, 5337 (2000).
- [20] U. R. Meza, B. S. Mendoza, and W. L. Mochán, *Phys. Rev. B* **99**, 125408 (2019).
- [21] Y. Furukawa, K. Kitamura, A. Alexandrovski, R. K. Route, M. M. Fejer, and G. Foulon, *Applied Physics Letters* **78**, 1970 (2001).
- [22] P. Giannozzi *et al.*, *Journal of Physics: Condensed Matter* **21**, 395502 (2009).
- [23] P. Giannozzi, O. Andreussi, T. Brumme, O. Bunau, M. B. Nardelli, M. Calandra, R. Car, C. Cavazzoni, D. Ceresoli, M. Cococcioni, N. Colonna, I. Carnimeo, A. D. Corso, S. de Gironcoli, P. Delugas, R. A. DiStasio, A. Ferretti, A. Floris, G. Fratesi, G. Fugallo, R. Gebauer, U. Gerstmann, F. Giustino, T. Gorni, J. Jia, M. Kawamura, H.-Y. Ko, A. Kokalj, E. Küçükbenli, M. Lazzeri, M. Marsili, N. Marzari, F. Mauri, N. L. Nguyen, H.-V. Nguyen, A. O. de-la Roza, L. Paulatto, S. Poncé, D. Rocca, R. Sabatini, B. Santra, M. Schlipf, A. P. Seitsonen, A. Smogunov, I. Timrov, T. Thonhauser, P. Umari, N. Vast, X. Wu, and S. Baroni, *Journal of Physics: Condensed Matter* **29**, 465901 (2017).
- [24] C. Attacalite and M. Grüning, *Phys. Rev. B* **88**, 235113 (2013).
- [25] F. Schmidt, A. L. Kozub, T. Biktajirov, C. Eigner, C. Silberhorn, A. Schindlmayr, W. G. Schmidt, and U. Gerstmann, *Phys. Rev. Research* **2**, 043002 (2020).
- [26] F. Schmidt, A. L. Kozub, U. Gerstmann, W. G. Schmidt, and A. Schindlmayr, *Crystals* **11** (2021).
- [27] A. Riefer, S. Sanna, A. Schindlmayr, and W. G. Schmidt, *Phys. Rev. B* **87**, 195208 (2013).
- [28] I. Shoji, T. Kondo, A. Kitamoto, M. Shirane, and R. Ito, *J. Opt. Soc. Am. B* **14**, 2268 (1997).
- [29] M. Trzeciecki, A. Dähn, and W. Hübner, *Phys. Rev. B* **60**, 1144 (1999).
- [30] R. C. Miller, *Applied Physics Letters* **5**, 17 (1964).
- [31] B. F. Levine, *Phys. Rev. B* **7**, 2600 (1973).
- [32] C. Merschjann, B. Schoke, D. Conradi, M. Imlau, G. Corradi, and K. Polgár, *Journal of Physics: Condensed Matter* **21**, 015906 (2008).
- [33] O. Beyer, D. Maxein, T. Woike, and K. Buse, *Appl. Phys. B* **83**, 527 (2006).
- [34] H. Badorreck, S. Nolte, F. Freytag, P. Bäune, V. Dieckmann, and M. Imlau, *Opt. Mater. Express* **5**, 2729 (2015).
- [35] E. K. Chang, E. L. Shirley, and Z. H. Levine, *Phys. Rev. B* **65**, 035205 (2001).
- [36] R. Leitsmann, W. G. Schmidt, P. H. Hahn, and F. Bechstedt, *Phys. Rev. B* **71**, 195209 (2005).
- [37] M. L. Trolle, G. Seifert, and T. G. Pedersen, *Phys. Rev. B* **89**, 235410 (2014).
- [38] A. Riefer and W. G. Schmidt, *Phys. Rev. B* **96**, 235206 (2017).
- [39] P. Deák, *Physica B: Condensed Matter* **535**, 35 (2018).
- [40] E. Cadelano, J. Furthmüller, G. Cappellini, and F. Bechstedt, *Journal of Physics: Condensed Matter* **26**, 125501 (2014).
- [41] S. Lyu and W. R. L. Lambrecht, *Phys. Rev. Materials* **2**, 124602 (2018).